

Defect identification in the  $\text{As}_{\text{Ga}}$  family in GaAs

H. Overhof\* and J.-M. Spaeth†

Department of Physics, University of Paderborn, Warburger Str. 100, D-33098 Paderborn, Germany

(Received 10 February 2005; revised manuscript received 7 April 2005; published 9 September 2005)

*Ab initio* total-energy calculations are presented for intrinsic defects in GaAs with a particular emphasis on hyperfine interactions in order to clarify the atomic structure of the various  $\text{As}_{\text{Ga}}$ -related defects. For the  $\text{As}_{\text{Ga}}\text{-X}_2$  defect complex the interpretation as an  $\text{As}_{\text{Ga}}\text{-V}_{\text{As}}$  antisite-vacancy pair as was considered so far is challenged. An  $\text{As}_{\text{Ga}}\text{-Ga}_{\text{As}}$  antistructure pair is the most likely identification. It is also unlikely that the  $\text{As}_{\text{Ga}}\text{-X}_1$  defect can be identified as a distant antistructure pair as was considered from magnetic resonance experiments. The theoretical results obtained for the isolated  $\text{As}_{\text{Ga}}$  point defect agree with the experimental data reported for the defect identified as isolated  $\text{As}_{\text{Ga}}$  and, with the exception of a small broadening of the nearest-neighbor lines and of a moderate splitting in the fifth shell, for the EL2 as well. We speculate that at room temperature the EL2 will be an isolated  $\text{As}_{\text{Ga}}$  defect which lowers its symmetry attracting some other mobile defect at the low temperatures required to perform magnetic resonance experiments. We have calculated the binding energies of antisites bound to a distant shallow acceptor and the influence of the pairing on the hyperfine interactions. We show that this mechanism could explain the broadening of the nearest-neighbor lines but not the splitting in the fifth shell.

DOI: 10.1103/PhysRevB.72.115205

PACS number(s): 71.15.Mb, 71.55.Eq, 76.30.Lh

## I. INTRODUCTION

The microscopic structure of the EL2 defect, the defect that determines the position of the Fermi level in semiinsulating GaAs, is still controversial (for a recent review, see Ref. 1).

Experimentally, at least four different  $\text{As}_{\text{Ga}}$ -related defects have been detected by optically detected magnetic resonance (ODMR) and optically detected electron-nuclear double resonance (ODENDOR), identified as the EL2 defect, the isolated  $\text{As}_{\text{Ga}}$  antisite, and the  $\text{As}_{\text{Ga}}\text{-X}_1$  and  $\text{As}_{\text{Ga}}\text{-X}_2$  pair defects. The hyperfine (hf) interactions for the isolated  $\text{As}_{\text{Ga}}$ , the  $\text{As}_{\text{Ga}}\text{-X}_1$ , and the EL2 are almost identical, whereas for the  $\text{As}_{\text{Ga}}\text{-X}_2$  pair the hf interactions are distinctly different.

The most interesting aspect of the members of the family of  $\text{As}_{\text{Ga}}$ -related defects is the metastability. Theoretical *ab initio* calculations<sup>2,3</sup> have shown that a large lattice relaxation of the  $\text{As}_{\text{Ga}}$  antisite is responsible for the defect metastability. Since in the metastable state the defect has been considered to be almost not observable, little theoretical effort has been spent to discriminate the metastable states of the different  $\text{As}_{\text{Ga}}$ -related defects. Recently, Chadi<sup>4</sup> has shown that the isolated  $\text{As}_{\text{Ga}}$  in its metastable state, the EL2M state, can have four different charge states, including two paramagnetic states.

The discrimination of the different  $\text{As}_{\text{Ga}}$ -related defects is difficult, because in GaAs all the host nuclei are paramagnetic: For Ga there are two isotopes (<sup>69</sup>Ga with 60.1% natural abundance has  $I=3/2$  and a nuclear  $g$  factor of 1.344 39, <sup>71</sup>Ga with natural abundance of 39.9%, also with  $I=3/2$  and a nuclear  $g$  factor of 1.708 18) while for As the <sup>75</sup>As nucleus, also with  $I=3/2$  has 100% natural abundance and a nuclear  $g$  factor of 0.959 647. Since the host nuclei are all paramagnetic and the gyromagnetic ratios are not small, the linewidth of the electron paramagnetic resonance (EPR) is large. Therefore the EPR spectrum of the  $\text{As}_{\text{Ga}}$ -related defects

shows just four lines from the hf interaction with the central <sup>75</sup>As<sub>Ga</sub> nucleus with  $I=3/2$ . More details are obtained from ODENDOR, but in all cases only the hf interaction with the central nucleus and the superhyperfine (shf) interactions with a few shells of neighbors can be resolved. The determination of the symmetry of these shells and the number of equivalent nuclei in a given shell is not always unequivocal.

While, with the exception of the  $\text{As}_{\text{Ga}}\text{-X}_2$  pair, the hf and shf interactions of these defects are very similar, the distinction between the different  $\text{As}_{\text{Ga}}$ -related defects has been made primarily on the basis of the magnetic circular dichroism of the absorption (MCDA).<sup>1,5</sup> The defect with an MCDA spectrum that is similar to the derivativelike structure expected for the optical transition between an  $A_1$  ground state and a  $T_2$  excited state of a tetrahedral impurity was identified to be the isolated tetrahedral  $\text{As}_{\text{Ga}}$ .<sup>5,6</sup> For this defect the EPR linewidth was somewhat smaller than for the other defects, which also show MCDA spectra that are more complex, as would be expected for a defect of lower symmetry.<sup>1</sup>

This, however, appears to be in conflict with the thermal stability of the defects: the isolated  $\text{As}_{\text{Ga}}$  defect is obtained by low-temperature electron irradiation of semi-insulating GaAs and disappears at room temperature,<sup>7</sup> when in electron irradiated material the  $\text{As}_{\text{Ga}}\text{-X}_1$  defect is observed. Finally, at  $T=520$  K the  $\text{As}_{\text{Ga}}\text{-X}_1$  defect disappears and the EL2 is dominant. This latter defect is quite stable, and it is the dominant defect in undoped liquid encapsulated Czochralski (LEC) crystals in a rather wide stoichiometric range  $0.48 < [\text{As}]/([\text{As}]+[\text{Ga}]) < 0.53$ .<sup>8,9</sup> The EL2 can be eliminated by a rapid quench from 1100 °C,<sup>10</sup> and is recovered by annealing the sample above 750 °C. If the EL2 is not the isolated antisite but some pair or complex with some other partner(s), its thermal stability indicates a strong binding to these partners while its paramagnetic properties strongly suggest the EL2 to be a nearly tetrahedral defect, for which the magnetization density is slightly disturbed in distant ligand shells only.

While we cannot solve this puzzle, we present in this paper *ab initio* calculations for several model systems consisting of one  $\text{As}_{\text{Ga}}$  antisite with other intrinsic defects, with a particular emphasis on the hf interactions. For the isolated antisite in its paramagnetic state we obtain a small symmetry-conserving relaxation only, in agreement with all computational results presented so far. Since the hf data obtained theoretically for this defect agree well with the experimental data, we conclude that for all  $\text{As}_{\text{Ga}}$ -related defects the relaxation is small, as otherwise the hf interactions would not show such a striking similarity. While we find a different identification for the  $\text{As}_{\text{Ga}}\text{-X}_2$  defect, an identification of the  $\text{As}_{\text{Ga}}\text{-X}_1$  defect and also of the EL2 cannot be presented. We show that a distant pair could account for the deviations of the hf interactions from those of the isolated  $\text{As}_{\text{Ga}}$  defect, but this pair cannot be identified with the EL2, nor with the  $\text{As}_{\text{Ga}}\text{-X}_1$ . Finally we consider pairing of the  $\text{As}_{\text{Ga}}$  antisite with distant shallow acceptors,  $\text{Zn}_{\text{Ga}}$  and  $\text{C}_{\text{As}}$ .

## II. COMPUTATION

Our total-energy Green's-function calculations make use of the linear muffin-tin orbital method in the atomic-spheres approximation (LMTO-ASA),<sup>11</sup> treating many-body effects within the local spin-density approximation of the density-functional theory (LSDA-DFT). For most calculations the band gap was corrected using the scissors operator technique (see e.g., Ref. 12). In our calculations, a perturbed region consisting of 29 atomic spheres (and 31 "empty spheres" to fill the space without undue overlap of the spheres) was embedded into an otherwise perfect infinite crystal. For isolated tetrahedral point defects a symmetry-conserving relaxation of the nearest neighbors was included to determine the lattice relaxation from the minimum of the total energy. Since our approach makes use of the ASA, its results are less reliable for lattice relaxations which exceed about 20% of a nearest-neighbor distance. For the paramagnetic states of the isolated intrinsic point defects the relaxations turned out to be small. We therefore have approximated the lattice relaxations for the pairs by the relaxations obtained for the isolated constituents. Pair binding energies are calculated from a comparison of the total energies of the constituents of the pair with the total energy of the pair itself. From the calculated magnetization densities the hf interactions have been calculated as described in Ref. 12.

## III. RESULTS

### A. Isolated $\text{As}_{\text{Ga}}$ point defect

For the neutral isolated  $\text{As}_{\text{Ga}}^0$  point defect we find a minimum of the total energy if the distance to the nearest-neighbors is increased by 4.7% with respect to the nearest-neighbor distance in the unperturbed crystal. The energy gained by this relaxation is 0.32 eV. A similar relaxation (4.0%, 0.33 eV energy gain) was reported by Dabrowski and Scheffler<sup>2</sup> for a 54 atom supercell calculation. For the defect in the singly positive charge state the relaxation reduces to 3% (1.4% for the double positive charge state). For the relaxed defects the calculated charge transition energies are

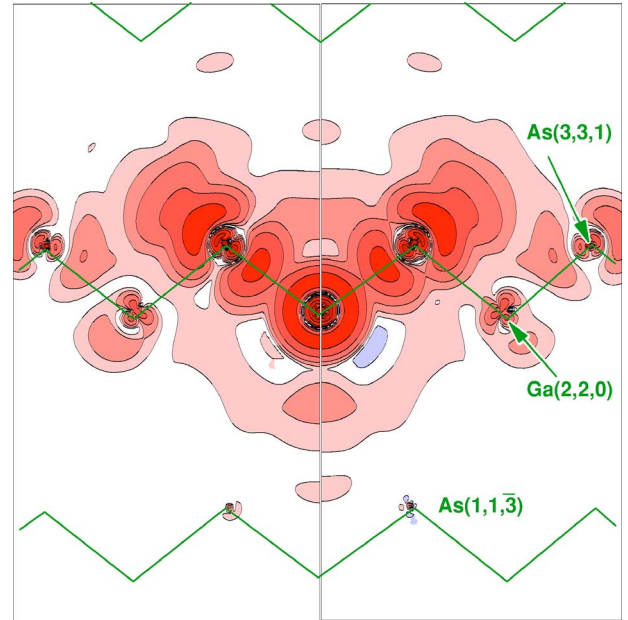


FIG. 1. (Color online) Contour plot of the magnetization density for the isolated  $\text{As}_{\text{Ga}}^+$  antisite in a  $(1\bar{1}0)$  plane in GaAs. The left panel shows the contribution of the gap state to the magnetization, the right part gives the total magnetization density. The Ga (As) lattice sites are at the lower (upper) side of the zigzag chain of nearest-neighbor bonds, respectively.

$E^{2+/+} = E_v + 0.98$  eV and  $E^{+/0} = E_v + 1.18$  eV, if the band gap is adjusted to the experimental value by the scissors operator (without this adjustment, the charge transition energies would be  $E_v + 0.37$  eV and  $E_v + 0.55$  eV, respectively). These values are somewhat smaller than the results (1.25 and 1.5 eV, respectively) obtained by Baraff and Schlüter<sup>13</sup> and by Delerue.<sup>14</sup> Note that these energies are significantly different from the charge transition energies ( $E_v + 0.54$  eV and  $E_v + 0.75$  eV, respectively) determined by Elliot *et al.* for the EL2.<sup>15</sup>

The effective potential of the  $\text{As}_{\text{Ga}}$  antisite is more attractive than that of the Ga lattice site. Therefore a gap state appears which transforms according to the  $a_1$  irreducible representation of the group  $T_d$ . For the twofold positive charge state of the antisite this state is unoccupied. The magnetization density for the paramagnetic  $\text{As}_{\text{Ga}}^+$  charge state shown in Fig. 1 is predominantly due to this gap state. The magnetization density is concentrated on the antisite, where it is  $s$  like, and its four nearest neighbors where it is predominantly  $p$  like. Similar to the case of elemental semiconductors,<sup>16</sup> the magnetization density is rather small at the  $(2, 2, 0)$  and  $(1, 1, \bar{3})$  neighbors, but again much larger at the more distant  $(3, 3, 1)$  neighbor. A comparison of the calculated hf interactions with experimental data reported by Krambock *et al.*<sup>6</sup> shows a close agreement already for the interactions that had been calculated without taking into account a lattice relaxation (see Table 8.9 of Ref. 12). The agreement is substantially improved if the lattice relaxation is included (see Table I). Note, however, that the agreement of the calculated data for the isolated  $\text{As}_{\text{Ga}}^+$  compared with experimental data for the EL2, e.g., is similar. In Table I we have listed the calcu-

TABLE I. Comparison of the experimental<sup>6</sup> hf and shf interaction data (in MHz) with calculated results for the 3% outward relaxed isolated  $\text{As}_{\text{Ga}}^+$  antisite in GaAs.

Ligand	$a/h$	$a_{\text{exp}}/h$	$b/h$	$b_{\text{exp}}/h$
$^{75}\text{As}_{\text{Ga}}^+$	2872.0	2650.0		
$^{75}\text{As}(1,1,1)$	171.2	169.3	46.7	53.2
$^{69}\text{Ga}(2,2,0)$	3.93		0.99	
$^{75}\text{As}(1,1,\bar{3})$	0.05		-0.20	
$^{69}\text{Ga}(4,0,0)$	2.57		0.10	
$^{75}\text{As}(3,3,1)$	22.3	21.5	4.15	2.2
$^{69}\text{Ga}(4,2,2)$	-0.95		-0.02	
$^{75}\text{As}(3,3,3)$	-0.12		0.02	

lated hf interactions with many shells of neighbors to demonstrate that there are larger interactions with the first and the fifth shell of neighbors only, whereas the shf interactions with all other shells are much smaller. In particular there are no larger interactions with the Ga nuclei, in agreement with the fact that these have not been detected by ODENDOR.

For the paramagnetic state of the isolated  $\text{As}_{\text{Ga}}^+$  the lattice relaxation is small (see also Ref. 2). Figure 2 shows the calculated total energy for the  $\text{As}_{\text{Ga}}^+$  defect as a function of the nearest-neighbor distance  $d$  for a relaxation that does not alter the tetrahedral defect symmetry. Also shown is the dependence of the hf interactions with the antisite nucleus and of the shf interactions with the nearest neighbors. As is the case for all deep donor states, the hf interaction with the donor nucleus is quite sensitively dependent on the nearest-neighbor distance. In our case, the moderate 3% outward

relaxation obtained for the minimum of the total energy leads to a 7% decrease of the hf interaction with the central nucleus (the same relaxation leads to a 9% decrease of the isotropic shf interaction and a 5% increase of the anisotropic shf interaction with the nearest-neighbor nuclei).

The magnitude of the calculated lattice relaxation is confirmed by the fact that the hf interactions calculated with this small lattice relaxation agree well with the experimental data. Since the hf interactions both with the central As nucleus and with the first shell of As ligands are strikingly similar for all members of the  $\text{As}_{\text{Ga}}$  family, we can safely exclude that the experimentally observed paramagnetic states of any members of the  $\text{As}_{\text{Ga}}$  family are subject to a major lattice relaxation of the  $\text{As}_{\text{Ga}}$  nucleus.

The metastability of the  $\text{As}_{\text{Ga}}$ -related defects is unequivocally described by a large trigonal lattice relaxation,<sup>2-4</sup> where the  $\text{As}_{\text{Ga}}$  antisite breaks a bond and moves in a  $[1, 1, 1]$  direction just beyond the plane formed by its three remaining neighbors. Due to this relaxation the  $p$ -like  $t_2$  resonance above the conduction-band edge splits into an  $a_1$  and an  $e$  state of the group  $C_{3v}$ , with the  $a_1$  state moving into the gap and eventually merging with the valence band, whereas the  $s$ -like  $a_1$  state of the undistorted antisite is not too much affected by the lattice distortion. In a recent paper Chadi<sup>4</sup> has shown that the  $\text{As}_{\text{Ga}}$  antisite in this EL2M distorted state can be stable in four different charge states ranging from positive to twofold negative. Due to our use of the ASA approximation in our LMTO-ASA treatment we cannot accurately describe the energetics of highly distorted defects, although we get a fair representation of the electron densities. The hf and shf interactions of the paramagnetic negative EL2M<sup>-</sup> state obtained by our approach differ not too much from those of the tetrahedral  $\text{As}_{\text{Ga}}^+$  state: The anisotropic interaction of the

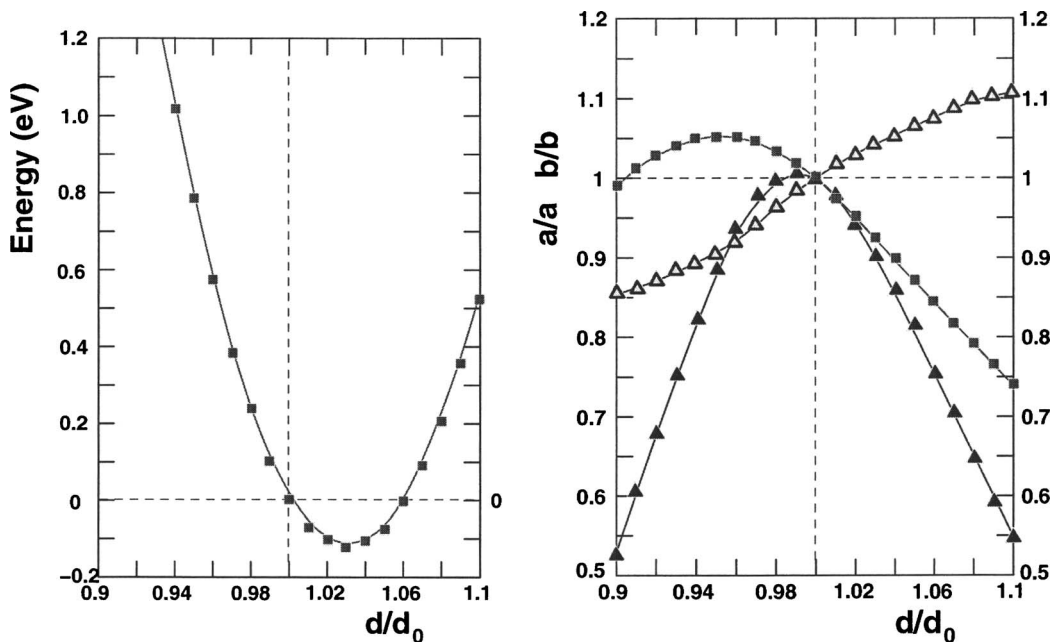


FIG. 2. Calculated total energy for the  $\text{As}_{\text{Ga}}^+$  antisite as a function of the nearest-neighbor distance  $d$ .  $d_0$  is the nearest-neighbor distance for the unrelaxed GaAs crystal (left). The right panel shows the change of hf interactions upon relaxation for the antisite normalized to its respective value without relaxation: contact interaction with the antisite nucleus (square) and contact (full triangle) and dipolar (open triangle) interactions with the nearest-neighbor nucleus.

TABLE II. Comparison of the experimental hf and shf interaction data (in MHz) for the  $\text{As}_{\text{Ga}}\text{-X}_2$  pair (Ref. 19) with calculated results for the trigonal  $(\text{As}_{\text{Ga}}\text{-Ga}_{\text{As}})^-$  antistructure pair in GaAs. Note: the experimental data for subshell IIb and IIc of Ref. 19 have been interchanged and shell IIb of Ref. 19 is reassigned to subshell Va.

Shell	$a_{\text{exp}}/h$	$b_{\text{exp}}/h$	$a/h$	$b/h$	$b'/h$	
0	2040	<50	2196	37		$^{75}\text{As}_{\text{Ga}}(0,0,0)$
Ia	$252 \pm 5$	$24 \pm 5$	259	39	0.4	$^{75}\text{As}(1, \bar{1}, \bar{1})$
Ib			7.2	11.5	0	$^{69}\text{Ga}_{\text{As}}(1,1,1)$
IIa			-11.0	0.5	0.01	$^{69}\text{Ga}(\bar{2}, \bar{2}, 0)$
IIb	$42.3 \pm 0.1$	$1.4 \pm 0.05$	39.7	2.4	0.9	$^{69}\text{Ga}(2,0,\bar{2})$
IIc	$\approx 17.0$	$\approx 0.6$	10.4	-0.4	0.4	$^{69}\text{Ga}(2,2,0)$
Va	$47.1 \pm 0.1$	$1.65 \pm 0.05$	22.1	1.5	0.02	$^{75}\text{As}(3,3,1)$

former defect are increased with respect to the latter state at the expense of the isotropic interactions. Furthermore, for the  $\text{EL2M}^-$  there are now prominent shf interactions with the next-nearest Ga nuclei. In contrast, the positive state of the  $\text{EL2M}^+$  has practically no isotropic hf interaction with the central  $\text{As}_{\text{Ga}}$  nucleus.

### B. $(\text{As}_{\text{Ga}}\text{-Ga}_{\text{As}})^-$ antistructure pair and the $\text{As}_{\text{Ga}}\text{-X}_2$ center

In contrast to the  $\text{As}_{\text{Ga}}$  antisite, the  $\text{Ga}_{\text{As}}$  antisite has a less attractive potential than the As lattice atom that it replaces. Due to this less attractive potential the valence states that transform according to the  $t_2$  irreducible representation are moved into the gap. According to our calculation the  $\text{Ga}_{\text{As}}$  antisite has charge states ranging from a single positive  $^4A_1$  state to a twofold negative  $^1A_1$  state, with transition energies in the lower half of the gap. In its negative charge state, the trigonal  $\{\text{As}_{\text{Ga}}(0,0,0)\text{-Ga}_{\text{As}}(1,1,1)\}^-$  antistructure pair with the antisites as nearest neighbors forms a paramagnetic  $^2A_1$  doublet state with a hf structure that is similar in many respects to that of the isolated  $\text{As}_{\text{Ga}}^+$ .

Table II displays the hf and shf data in comparison with experimental data for the  $\text{As}_{\text{Ga}}\text{-X}_2$  defect complex.<sup>17</sup> Experimentally, the hf structure of the  $\text{As}_{\text{Ga}}\text{-X}_2$  defect is unique within the  $\text{As}_{\text{Ga}}$  defect family in several respects: the contact interaction with the central  $^{75}\text{As}$  nucleus is 20% smaller than for the other paramagnetic  $\text{As}_{\text{Ga}}$ -related defects, the shf interactions with nearest  $^{75}\text{As}$  ligand nuclei are nearly 50% larger for the isotropic shf interactions, but smaller by a factor of 2 for the dipolar interactions if compared with the corresponding interactions for the other members of the  $\text{As}_{\text{Ga}}$  family. The orientations of the shf tensor axes for this ligand shell deviate strongly from the tetrahedral orientations found for the other  $\text{As}_{\text{Ga}}$ -related defects. Finally, for the  $\text{As}_{\text{Ga}}\text{-X}_2$  defect complex the hf interactions with two shells of Ga nuclei have been detected. Note that interactions with a Ga nucleus had not been resolved experimentally for the isolated  $\text{As}_{\text{Ga}}^+$ , nor for the EL2.

The  $\text{As}_{\text{Ga}}\text{-X}_2$  defect had originally been interpreted as a  $\text{As}_{\text{Ga}}\text{-V}_{\text{As}}$  antisite-vacancy pair<sup>18</sup> and later been re-interpreted as the negatively charged and trigonally distorted  $\text{As}_{\text{Ga}}^-$

defect.<sup>25</sup> A careful analysis of the ODMR linewidth<sup>17,19</sup> has shown that the first shell of As neighbors consists of three members only, suggesting a trigonal pair. From the amplitude of the forbidden MCDA-EPR transitions a large quadrupole interaction with the central nucleus was inferred, which would be incompatible with a tetrahedral site and strongly indicates the presence of another charged defect as nearest neighbor to the  $\text{As}_{\text{Ga}}$  central defect.

This second defect, which should be an intrinsic defect, had not been observed in magnetic resonance. Since all intrinsic defects in GaAs are either vacancies or have a non-zero nuclear spin, it was assumed that most likely a  $\text{V}_{\text{As}}$  vacancy is in the first As ligand shell and therefore the  $\text{As}_{\text{Ga}}\text{-X}_2$  defect was identified<sup>19</sup> as a nearest-neighbor  $\text{As}_{\text{Ga}}\text{-V}_{\text{As}}$  antisite-vacancy pair. We shall show in Sec. III B that this identification cannot be maintained according to our results. Instead, we identify the  $\text{As}_{\text{Ga}}\text{-X}_2$  defect with a  $(\text{As}_{\text{Ga}}\text{-Ga}_{\text{As}})^-$  nearest-neighbor antistructure pair. This new assignment shares with the previous assignment that it also provides three As ligands in the first shell of ligands with a twofold negatively charged defect being the fourth neighbor of the  $\text{As}_{\text{Ga}}$  center.

The hf interactions calculated for the  $(\text{As}_{\text{Ga}}\text{-Ga}_{\text{As}})^-$  antistructure pair are compared with experimental data from Ref. 19 in Table II. From the analysis of experimental ODENDOR lines it is not possible to infer the distance of the nuclei (shells) measured from the central nucleus. Therefore the assignment of lines to subshells must remain tentative without a theoretical interpretation (see also Ref. 12). When comparing experimental and theoretical hf and shf interaction data we therefore do not follow the assignment of the subshells given by Ref. 19, which had been made on the basis of the tensor angles only.

We propose instead to interchange the assignment of shells IIb and IIc in the experimental data and to replace IIIb by Va. The latter change is proposed not just to improve the agreement between theory and experiment, but considering that for most deep donor states the shf interactions with shell V are larger than with nuclei of shell III.<sup>16</sup>

With this identification we find a very good agreement of the calculated shf interactions with the experimental data for all shells for which a comparison is possible. Quite unex-

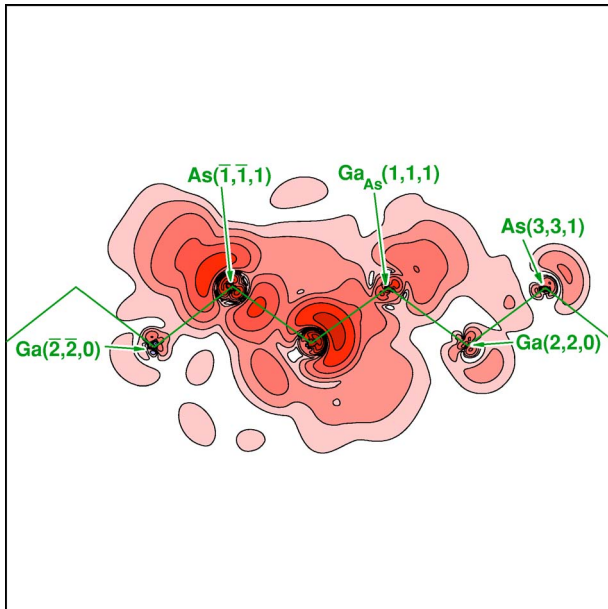


FIG. 3. (Color online) Contour plot of the magnetization density for the trigonal  $\{\text{As}_{\text{Ga}}(0,0,0)\text{-Ga}_{\text{As}}(1,1,1)\}^-$  antistructure pair in GaAs.

pectedly, the shf interactions with the  $\text{Ga}_{\text{As}}$  antisite nucleus are of the order of 10 MHz only. Since the hf interaction is small and very anisotropic, it is not astonishing that it is not resolved in the ODENDOR experiment. Furthermore, the striking differences between the experimental shf interactions for the isolated  $\text{As}_{\text{Ga}}$  point defect and for the  $\text{As}_{\text{Ga}}\text{-X}_2$  defect pair are well reproduced by the results calculated for the  $(\text{As}_{\text{Ga}}\text{-Ga}_{\text{As}})^-$  antistructure pair. For this pair we obtain the charge transfer energy  $E^{0/-} = E_v + 1.47$  eV, reasonably close to the value of 1.2 eV reported by Koschnick *et al.*<sup>1</sup> for the corresponding level for the  $\text{As}_{\text{Ga}}\text{-X}_2$  center.

Figure 3 illustrates the results of Table II: the magnetization density is concentrated at the  $\text{As}_{\text{Ga}}$  nucleus and its nearest-neighbor (NN) As ligands, but much smaller in the vicinity of the  $\text{Ga}_{\text{As}}$  ligand. For the antistructure pair in its paramagnetic negative charge state the binding is predominantly electrostatic between a singly positive  $\text{As}_{\text{Ga}}^+$  and a doubly negative  $\text{Ga}_{\text{As}}^{2-}$  antisite. The calculated value of 1.3 eV for the pair binding energy is consistent with this interpretation and also with the reported thermal stability of the pair.<sup>1</sup>

#### The $\text{As}_{\text{Ga}}\text{-V}_{\text{As}}$ pair

According to our calculation, which generally agrees with the earlier calculation of Delerue,<sup>14</sup> the isolated neutral tetrahedral  $\text{V}_{\text{As}}^0$  vacancy has a  $^4A_1$  high-spin state that originates from three  $t_2$  spin-up dangling-bond-like gap states. Forming a trigonal pair these states are split into  $a_1$  and  $e$  states of the group  $C_{3v}$ . The interaction of the dangling-bond  $a_1$  state with the  $\text{As}_{\text{Ga}}$ -related  $a_1$  state gives rise to hybridized bonding and antibonding  $a_1$  linear combinations. In the 2+ charge state of the pair the lower  $a_1$  single particle state is occupied by one electron that gives rise to an  $^2A_1$  state. Since the lower  $a_1$  state is predominantly dangling-bond like, its isotropic hf interaction with the  $^{75}\text{As}_{\text{Ga}}$  nucleus amounts to 390 MHz

only, a factor of 5 smaller than required to be taken as the interaction with the defect center nucleus observed for  $\text{As}_{\text{Ga}}\text{-X}_2$ . Furthermore, the shf interactions with the other ligands also do not fit into the pattern determined experimentally. The occupation of the upper  $a_1$  single-particle state (which in fact would give a hf interaction that agrees with the experimental value for  $\text{As}_{\text{Ga}}\text{-X}_2$ ) would require that the four  $e$  single-particle states are also occupied, which would correspond to a fourfold negative charge state of the pair. According to our results, the singly negative charge state of the pair is already the state with the highest possible electron occupation.

Alternatively we could attempt to invert the term order assuming a strong lattice relaxation for the pair: assuming a relaxation of the antisite away from the vacancy position (according to our calculation and to Pöykkö *et al.*<sup>20</sup> the relaxation should occur in the opposite direction), the lower  $a_1$  state moves toward the upper  $a_1$  state, but due to the stronger hybridization of the two  $a_1$  states the isotropic hf interaction derived from each  $a_1$  state is smaller by about a factor of 2 than the experimental value for  $\text{As}_{\text{Ga}}\text{-X}_2$ . In contrast, a relaxation as predicted by our calculation and by Pöykkö *et al.*<sup>20</sup> even increases the discrepancy observed for the unrelaxed pair. As noted above, the similarity of the hf interactions of all members of the  $\text{As}_{\text{Ga}}$  family is a strong argument that at least the paramagnetic states are not subject to a major lattice relaxation in the central region of the defect.

The result for the  $\text{As}_{\text{Ga}}\text{-V}_{\text{As}}(\text{NN})$  pair demonstrates that by *ab initio* calculations of hf interactions it is often quite easy to falsify a defect model. This falsification is even more convincing, if (as in the present case) with the  $(\text{As}_{\text{Ga}}\text{-Ga}_{\text{As}})^-$  pair an alternative model can be presented that fits perfectly into the experimental data. The present results further demonstrate that a defect nucleus can be invisible in ODENDOR, even if this nucleus is paramagnetic with a 100% natural abundance, if this nucleus has shf interactions that are too small to give rise to enough line intensities to be observed.

#### C. $\text{As}_{\text{Ga}}\text{-Ga}_{\text{As}}(\text{NNN})$ antistructure pair and the $(\text{As}_{\text{Ga}}\text{-X}_1)$ center

The  $\text{As}_{\text{Ga}}\text{-X}_1$  defect was identified by Krambrock and Spaeth<sup>5</sup> as  $\text{As}_{\text{Ga}}\text{-Ga}_{\text{As}}(\text{NNN})$  pair. The presence of a  $\text{Ga}_{\text{As}}$  antisite was concluded from the hf interaction with a single Ga nucleus detected by ODENDOR. It was further concluded that the  $\text{Ga}_{\text{As}}$  antisite cannot be at the nearest-neighbor position to the  $\text{As}_{\text{Ga}}$  antisite, as in this case there would be only three As ligands to the  $\text{As}_{\text{Ga}}$  antisite, which would be in conflict with the EPR linewidth.

If we place the  $\text{As}_{\text{Ga}}$  antisite in the origin, then the second As shell would be at  $(1,1,\bar{3})$ . The antistructure pair with these coordinates in  $C_s$  symmetry has a very small pair binding energy  $E_{\text{bind}} = 0.2$  eV. The gap states depicted in Fig. 4 are practically the unaltered superimposed gap states of the isolated  $\text{As}_{\text{Ga}}$  and  $\text{Ga}_{\text{As}}$  point defects. In a similar way the induced density-of-states (DOS) distribution, i.e., the change of the DOS upon introduction of the defect pair, is a mere superposition of the induced DOS distributions of the iso-

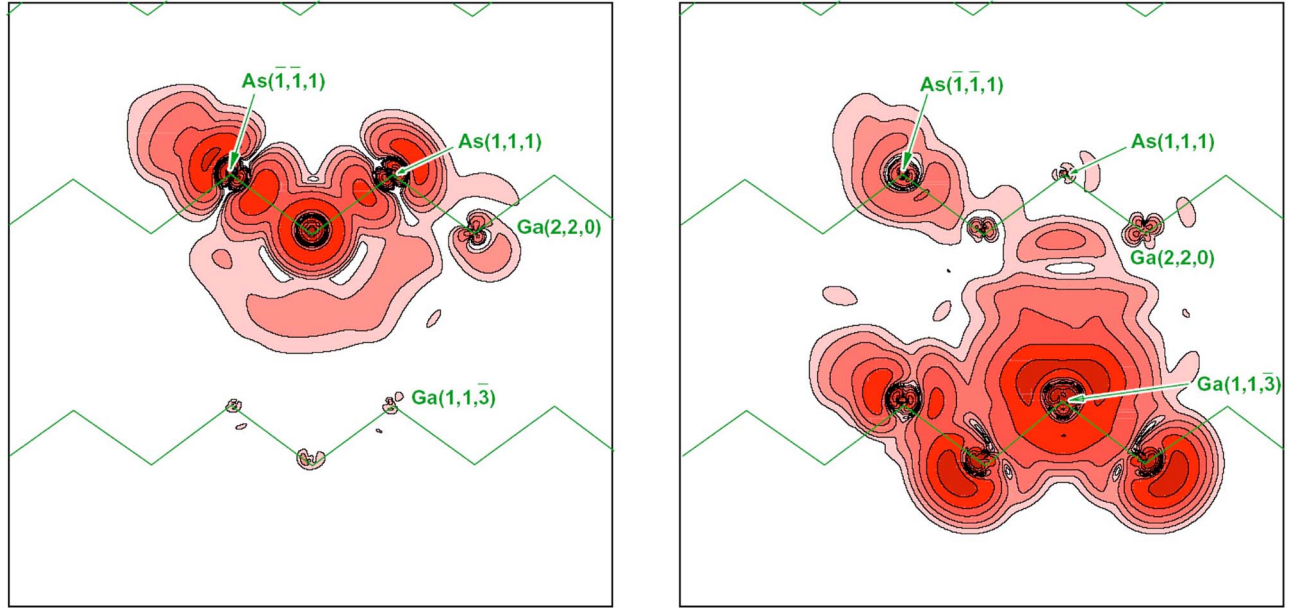


FIG. 4. (Color online) Contour plot of the particle densities for the distant  $\{\text{As}_{\text{Ga}}(0,0,0)\text{-Ga}_{\text{As}}(1,1,\bar{3})\}^-$  antistructure pair in GaAs. The left panel shows the total magnetization density, the right panel gives the particle density of the lower gap states that originate from the former  $t_2$  gap state.

lated partners. When comparing the hf interactions calculated for this  $\text{As}_{\text{Ga}}\text{-Ga}_{\text{As}}(\text{NNN})$  pair with the ODENDOR results for  $\text{As}_{\text{Ga}}\text{-X}_1$ ,<sup>5</sup> we find some similarity, although the details of the splitting in the subshells are somewhat different (see Table III). These deviations could of course be caused by our approximation of the lattice relaxation inserting the values obtained for the constituents of the pair in tetrahedral symmetry. Unfortunately, our present code does not provide us with sufficiently accurate relaxation energies for low-symmetry relaxations.

The identification of the  $\text{As}_{\text{Ga}}\text{-X}_1$  as  $\text{As}_{\text{Ga}}\text{-Ga}_{\text{As}}(\text{NNN})$  antistructure pair rested on the observation of the hf interaction with a single Ga nucleus.<sup>5</sup> In our calculation, we also find a hf interaction with a Ga nucleus, which happens to agree in magnitude with the value observed experimentally. But this interaction is due to the  $\text{Ga}(0,2,\bar{2})$  nuclei which in  $C_s$  sym-

metry form a shell of two equivalent nuclei, while for the shf interaction with the Ga antisite nucleus we find a value that is below the experimental resolution (see Table III). Since in the experiments the interaction with a *single* Ga nucleus is observed (in 12 orientations of the defect as is appropriate for the  $C_s$  symmetry), this defect cannot be identified with the  $\text{As}_{\text{Ga}}\text{-Ga}_{\text{As}}(\text{NNN})$  antistructure pair.

We have considered the effect of additional lattice relaxations around the  $\text{Ga}_{\text{As}}$  antisite, but the spin density at the antisite nucleus was not sensitive to small relaxations.

We have investigated two additional antistructure pairs, a pair of  $C_s$  symmetry where the  $\text{Ga}_{\text{As}}$  antisite is in shell V at  $(3,3,1)$ , and a trigonal pair, where it is at  $(3,3,3)$ . For the former pair we have virtually no pair binding energy. However, as the magnetization density of the isolated  $\text{As}_{\text{Ga}}$  defect is relatively large at the  $(3,3,1)$  site (see Fig. 1 and Table I),

TABLE III. Comparison of the experimental hf and interaction data (Ref. 19) (in MHz) for the  $\text{As}_{\text{Ga}}\text{-X}_1$  pair with calculated results for the relaxed  $\{\text{As}_{\text{Ga}}(0,0,0)\text{-Ga}_{\text{As}}(1,1,\bar{3})\}^-$  antistructure pair in GaAs. Note that for the pair with  $C_s$  symmetry the  $^{75}\text{As}(1, \bar{1}, 1)$  and the  $^{69}\text{Ga}(0,2,\bar{2})$  shells contain two members.

Shell	$a_{\text{exp}}/h$	$b_{\text{exp}}/h$	$a/h$	$b/h$	$b'/h$	Shell
$^{75}\text{As}_{\text{Ga}}(0,0,0)$	2600.0		2724.0	0.16	0.09	$^{75}\text{As}_{\text{Ga}}(0,0,0)$
NN As shell						
nucleus 1	158.5	54.7				
nuclei 2-4	205.4	50.8				
			195.0	47.0	1.0	$^{75}\text{As}(1,1,1)$
			181.0	45.0	0.01	$^{75}\text{As}(\bar{1},\bar{1},1)$
			173.0	45.0	1.6	$^{75}\text{As}(1,\bar{1},\bar{1})$
$^{69}\text{Ga}_{\text{As}}$	22.5	1.9	-1.14	0.22	0.17	$^{69}\text{Ga}_{\text{As}}(1,1,\bar{3})$
			20.6	0.8	0.7	$^{69}\text{Ga}(0,2,\bar{2})$

we observe a significant perturbation of the  $\text{As}_{\text{Ga}}$ -derived magnetization density caused by the  $\text{Ga}_{\text{As}}$  antisite. We therefore find isotropic shf interactions with several shells of  $^{69}\text{Ga}$  nuclei [including the  $\text{Ga}_{\text{As}}(3,3,1)$  antisite] in the 20–45-MHz range. Furthermore, the isotropic shf interactions calculated for the three subshells of the nearest-neighbor shell range from 56 to 237 MHz, much more than observed experimentally. For the distant trigonal pair we obtain a binding energy of 0.1 eV, and a splitting of the shf interactions for the As nuclei in the first neighbor shell that is with 10% about 1/2 of the value observed experimentally. The shf interaction with the  $^{69}\text{Ga}_{\text{As}}(3,3,1)$  antisite nucleus is close to zero, a significant hf interaction with Ga nuclei is found for the  $^{69}\text{Ga}_{\text{As}}(2,2,0)$  shell only. Here the shf interaction  $a=9.5$  MHz cannot be identified with the Ga interaction found experimentally, because it is with a shell of three equivalent nuclei.

In conclusion, we have not found an antistructure pair that shows a hf interaction with a single Ga nucleus as is observed for  $\text{As}_{\text{Ga}}\text{-X}_1$ . We have obtained shf interactions with  $^{69}\text{Ga}$  ligand nuclei which are of the correct order of magnitude, but these are not the shf interactions with the  $\text{Ga}_{\text{As}}$  antisite nucleus.

#### D. EL2 defect

The first observation of the EL2 by EPR (Ref. 21) showed the defect to be caused by an  $\text{As}_{\text{Ga}}$  antisite defect. In its neutral state, the diamagnetic  $\text{EL2}^0$  defect was attributed to an isolated tetrahedral  $\text{As}_{\text{Ga}}$  defect from the uniaxial stress dependence of its zero-phonon line and their phonon replica.<sup>8,22</sup> From MCDA-EPR experiments Meyer *et al.*<sup>23</sup> concluded that the paramagnetic  $\text{EL2}^+$  cannot be identified with the isolated  $\text{As}_{\text{Ga}}^+$ . From DLTS and EPR experiments the EL2 defect was concluded to be a trigonal  $\text{As}_{\text{Ga}}\text{-As}_i$  pair,<sup>24,27</sup> and Meyer *et al.*<sup>26</sup> observed by MCDA-ENDOR an additional As nucleus and concluded that EL2 is to be identified with a distant trigonal  $\text{As}_{\text{Ga}}\text{-As}_i$  antisite-interstitial pair. From total-energy calculations,<sup>2</sup> however, such a pair was concluded to be quite unlikely because of its small pair binding energy.

By *ab initio* total-energy calculations the metastability of the EL2 defect was explained assuming the paramagnetic  $\text{EL2}^+$  defect to be identified with the isolated tetrahedral  $\text{As}_{\text{Ga}}^+$  antisite<sup>2,3</sup> without the need of inducing an  $\text{As}_i$  interstitial. Furthermore, the presence of an interstitial was questioned by Wirbeleit and Niklas<sup>28</sup> from an analysis of the EPR linewidth using an improved scheme for the computation of the line positions of the many pseudodipolar coupled nuclear spins. Finally, Tkach *et al.*<sup>29</sup> have re-investigated the EL2 using MCDA-EPR in the W band (95 GHz). With the higher magnetic field in the W band the Zeeman splittings are much larger than the hf interactions and therefore the pseudodipolar coupling is absent in the ENDOR lines. From the high-field ENDOR the presence of an  $\text{As}_i$  nucleus in the EL2 defect can be excluded. The observed hf interactions are almost compatible with an isolated tetrahedral  $\text{As}_{\text{Ga}}^+$  defect, except for an increased linewidth of the hf interactions in the nearest-neighbor shell which might indicate a 1.5% splitting

of these interactions and a resolved splitting of the interactions that were ascribed to shell V.

This experimental result raises some problems which cannot be answered properly. The increased linewidth and the splitting observed for shell V strongly suggests that at least a partner to the  $\text{As}_{\text{Ga}}^+$  is present in the EL2. Since the EL2 is stable up to 800 K, the pair must be tightly bound by at least 2 eV and, since the EPR linewidth is the same as for the isolated  $\text{As}_{\text{Ga}}^+$ , the partner cannot be at the nearest-neighbor substitutional position. It must not be an intrinsic interstitial, as both  $\text{As}_i$  and  $\text{Ga}_i$  could not stay unobserved. If such a pair was covalently bound by 2 eV, a drastic change of the bonds of its constituents would be expected. As these necessarily influence the paramagnetic states (even if these are antibonding, they must be orthogonal on the bonding states and should be affected by the change of the orthogonalization), it is quite unlikely that the shf interactions with the nearest neighbors are affected by some 1.5% only. From the above it follows that the EL2 must not be a covalently bound pair.

A binding of the pair by Coulomb forces would require that the partner to the paramagnetic  $\text{As}_{\text{Ga}}^+$  is negatively charged (highly charged in fact to give rise to a binding energy of 2 eV), making the EL2 an acceptor. But the technological relevance of the EL2 rests on its property as a double donor.

We therefore should consider that the EL2 at normal temperatures is identical with the isolated tetrahedral  $\text{As}_{\text{Ga}}$  point defect. When cooling the samples to helium temperature, compensating mobile acceptors may migrate and bind to the  $\text{As}_{\text{Ga}}$  point defect by Coulomb forces, causing the increased linewidth and the splittings observed in shell V. This might also be a possible explanation for the  $\text{As}_{\text{Ga}}\text{-X}_1$  defect.

#### 1. Distant orthorhombic $\{\text{As}_{\text{Ga}}(0,0,0)\text{-V}_{\text{Ga}}(0,0,4)\}^{2-}$ antisite-vacancy pair

In order to show that in principle a distant pair bound moderately by Coulomb forces could explain the properties observed for the EL2, we have calculated a model where the antisite is separated from the vacancy by a full lattice constant along the cubic axis.<sup>30</sup> This ensures that the properties of the pair are similar to those of the isolated antisite as is revealed by the hf interaction data listed in Table IV. The pair formation energies are rather small: we obtain 0.34 eV for the singly negative pair, and 0.3 eV for the threefold negative pair if we relax the ligands of the  $\text{As}_{\text{Ga}}$  and of the  $\text{V}_{\text{Ga}}$  as for the isolated trigonal defects (there are no common ligands for the constituents of the pair). These pair binding energies are considerably smaller than the electrostatic energies expected for a  $\{\text{As}_{\text{Ga}}(0,0,0)^+\text{-V}_{\text{Ga}}(0,0,4)^{3-}\}$  pair (0.8 eV), which in the  $\{\text{As}_{\text{Ga}}(0,0,0)^{2+}\text{-V}_{\text{Ga}}(0,0,4)^{3-}\}$  charge state corresponding to  $\text{EL2}^+$  which with 1.6 eV would be sufficient to ensure the observed stability of the pair. Obviously the polarization of the crystal surrounding the defect pair screens the charges much more effectively than the long-range screening which is given by the electrostatic dielectric constant.

The charge transfer energies are found to be  $E^{2-/} = E_v + 1.18$  eV and  $E^{2-/\beta-} = E_v + 1.49$  eV, respectively. The charge states of the pair are quite different from those of the

TABLE IV. Comparison of the experimental hf interaction data (in MHz) for the EL2 defect with calculated results for the unrelaxed  $\{\text{As}_{\text{Ga}}(0,0,0)-\text{V}_{\text{Ga}}(0,0,4)\}^{2-}$  defect pair in GaAs.

Shell	$a_{\text{exp}^+}/h$	$b_{\text{exp}^+}/h$	$a/h$	$b/h$
$^{75}\text{As}_{\text{Ga}}(0,0,0)$	$2656. \pm 15$		3056.0	-0.15
$^{75}\text{As}(1,1,1)$			190.5	44.1
	$170.5 \pm 0.4$	$54.3 \pm 0.4$		
$^{75}\text{As}(1, \bar{1}, \bar{1})$			198.3	43.23
Shell	$A_{\text{exp}^+}(0,0,1)/h$		$a/h$	$b/h$
			31-36	
			39-42	
$^{75}\text{As}(3,3,1)$			31.0	3.5
$^{75}\text{As}(3, \bar{3}, \bar{1})$			33.2	3.7

isolated defects, primarily because in semi-insulating and in  $n$ -type material the  $\text{V}_{\text{Ga}}$  is in the  $(3-)$  charge state.

Table IV compares the hf and shf interaction data for the EL2 defect with those calculated for the unrelaxed orthorhombic  $\{\text{As}_{\text{Ga}}(0,0,0)-\text{V}_{\text{Ga}}(0,0,4)\}^{2-}$  pair. The agreement is satisfactory in the sense that perfect agreement does not seem unlikely if a correct lattice relaxation could be implemented. It should be noted, however, that the splitting of shell of nearest neighbors into two subshells leads to isotropic shf interactions that differ by 4%, three times the value estimated by Tkach *et al.*<sup>29</sup> from the increased linewidth. It thus seems that the pair distance of one lattice constant leads to a pair that is still bound too tightly to fully account for the small splitting of the shf interactions for the shell of nearest neighbors.

It is interesting to compare the magnetization density of this pair (see Fig. 5) with that calculated for the isolated  $\text{As}_{\text{Ga}}^+$  point defect in Fig. 1. There are hardly any

differences—the  $\text{V}_{\text{Ga}}^{3-}$  partner represents a strong Coulombic attraction for  $\text{As}_{\text{Ga}}^+$ , but since it is diamagnetic it only minutely influences the magnetization density. In contrast, the induced electron density shows the strong influence of the  $\text{V}_{\text{Ga}}^{3-}$  on the electron density of the pair.

## 2. Pairing of the $\text{As}_{\text{Ga}}^+$ antisite with shallow acceptors

For the EL2 we have speculatively proposed that this defect is an isolated antisite which forms a complex with some mobile partner upon cooling to temperatures well below room temperature. Since the paramagnetic state of the EL2 requires compensating acceptors, it appears likely that shallow acceptors are involved. We have compared the total energies of pairs of the  $\text{As}_{\text{Ga}}^+$  antisite with shallow acceptors with the sum of the total energies of the constituents of the pairs. As examples for shallow acceptors on both sublattices we have chosen the  $\text{Zn}_{\text{Ga}}^-$  and  $\text{C}_{\text{As}}^-$  acceptors. Table V shows the pair binding energy  $\Delta E$  for various separations of

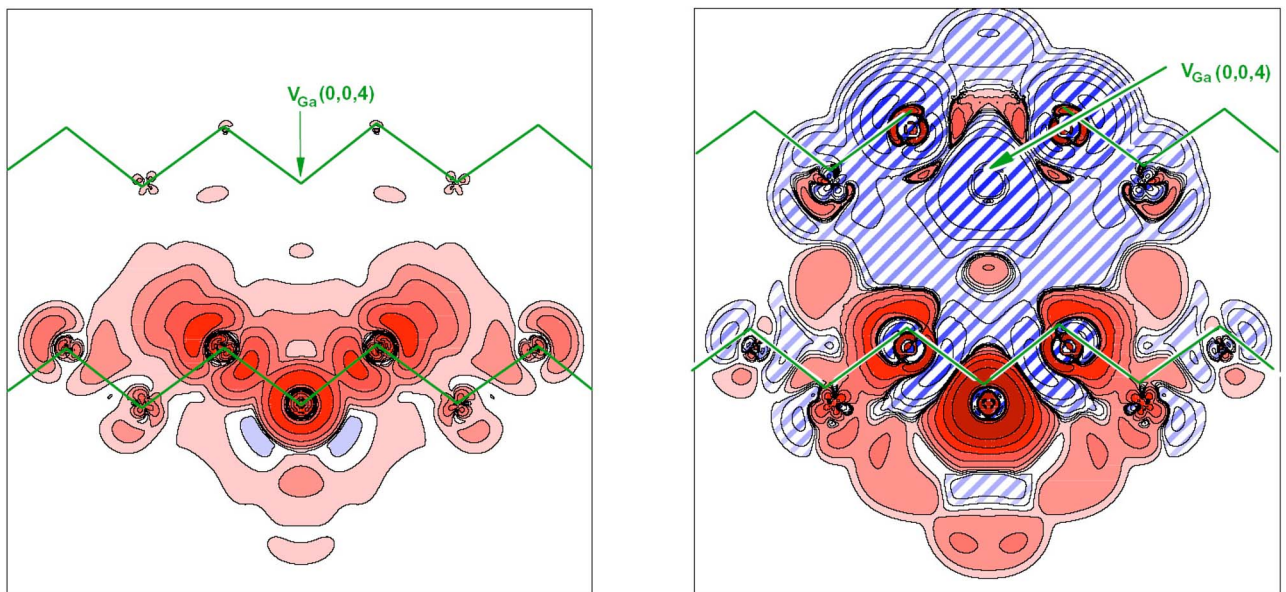


FIG. 5. (Color online) Contour plot of the magnetization density (left) and of the total induced electron density (right) for the orthorhombic  $\{\text{As}_{\text{Ga}}(0,0,0)-\text{V}_{\text{Ga}}(0,0,4)\}^{2-}$  pair in GaAs.

TABLE V. Pair binding energy  $\Delta E$  (in eV) for pairs of the  $\text{As}_{\text{Ga}}^+$  antisite with  $\text{Zn}_{\text{Ga}}^-$  and  $\text{C}_{\text{As}}^-$  acceptors at different distances. Also listed is the variation  $\Delta a/h$  (in MHz) of the isotropic shf interactions with the nearest-neighbor  $^{75}\text{As}$  ligand nuclei.

Pair	$\Delta E$	$\Delta a/h$
$\text{As}_{\text{Ga}}(0,0,0)\text{-Zn}_{\text{Ga}}(2,2,0)$	0.228	75.9
$\text{As}_{\text{Ga}}(0,0,0)\text{-Zn}_{\text{Ga}}(0,0,4)$	0.054	1.32
$\text{As}_{\text{Ga}}(0,0,0)\text{-Zn}_{\text{Ga}}(2,2,4)$	0.051	4.18
$\text{As}_{\text{Ga}}(0,0,0)\text{-Zn}_{\text{Ga}}(4,4,4)$	0.011	1.31
$\text{As}_{\text{Ga}}(0,0,0)\text{-C}_{\text{As}}(1,1,1)$	0.942	
$\text{As}_{\text{Ga}}(0,0,0)\text{-C}_{\text{As}}(1,1,\bar{3})$	0.079	11.8
$\text{As}_{\text{Ga}}(0,0,0)\text{-C}_{\text{As}}(3,3,1)$	0.146	100.8
$\text{As}_{\text{Ga}}(0,0,0)\text{-C}_{\text{As}}(3,3,3)$	0.020	8.2
$\text{As}_{\text{Ga}}(0,0,0)\text{-C}_{\text{As}}(5,5,1)$	0.077	24.6
$\text{As}_{\text{Ga}}(0,0,0)\text{-C}_{\text{As}}(5,5,5)$	0.022	0.05

the constituents of the pair. In contrast to a simple electrostatic model  $\Delta E$  is not a monotonic function of the intrapair separation; the binding energy  $\Delta E$  is relatively large if the acceptor is located at a position where the electron density of the isolated antisite would be large, at the (3,3,1) and the (5,5,1), positions, e.g., but rather small at positions where this electron density is small [at (0,0,4), e.g.].

For all pairs with an intrapair separation exceeding two nearest-neighbor distances the hf interaction with the central antisite nucleus is within computational accuracy identical with that obtained for the isolated antisite. The same is true for the mean value of the isotropic and anisotropic shf interactions with the nuclei of the nearest-neighbor  $^{75}\text{As}$  ligand shell. Since pairing lifts the symmetry of the pair, the shf interactions with the nearest-neighbor  $^{75}\text{As}$  nuclei are not identical but show some variation,  $\Delta a/h$ . For pairs with larger binding energies this variation  $\Delta a/h$  exceeds 10 MHz even for the pairs with rather large interpair separations.

For the pairs with shallow acceptors to be identified with the defect that gives rise to the EL2 spectra the variation  $\Delta a/h$  must be below about 2 MHz (see Ref. 29) in order to account for the increased linewidth. Note that for the pairs with shallow  $\text{Zn}_{\text{Ga}}^-$  acceptors this condition [with the exception of the  $\text{As}_{\text{Ga}}(0,0,0)\text{-Zn}_{\text{Ga}}(2,2,0)$  pair] is nearly met, while for the  $\text{C}_{\text{As}}^-$  acceptors this condition is not met for pairs with large intrapair separations. Thus it appears not unlikely that the paramagnetic  $\text{EL2}^+$  is the neutral pair of an  $\text{As}_{\text{Ga}}^+$  antisite with rather distant and weakly bound shallow acceptors on the Ga sublattice. We must, however, admit that we cannot check our model comparing the shf data for the fifth ligand shell, for which only incomplete experimentally determined shf interactions are available:<sup>29</sup> Since there are no angular dependent ODENDOR spectra experimental, the experimental data cannot be analyzed, and for the low-symmetry pairs our present code does not allow us to calculate shf interactions for *all* subshells of a distant shell.

It should be noted that the hf and shf interactions of the  $\text{As}_{\text{Ga}}(0,0,0)\text{-C}_{\text{As}}(1,1,1)$  pair are quite different from those of the  $\text{As}_{\text{Ga}}\text{-X}_2$  pair: the hf interaction with the central nucleus in the  $\text{As}_{\text{Ga}}(0,0,0)\text{-C}_{\text{As}}(1,1,1)$  pair is hardly different from that of the isolated  $\text{As}_{\text{Ga}}^+$  and also the shf interactions with the three  $^{75}\text{As}$  nearest-neighbor ligands do not show the striking difference to those of the isolated antisite which are typical for the  $\text{As}_{\text{Ga}}\text{-X}_2$  pair.

#### IV. CONCLUSIONS

The agreement of the calculated hf interactions for the isolated  $\text{As}_{\text{Ga}}$  with the experimental ODENDOR data indicates that the theoretical method describes the hf and shf interactions for this defect quite accurately. For the  $\text{As}_{\text{Ga}}\text{-X}_2$  we find that the proposed model as a nearest-neighbor  $\text{As}_{\text{Ga}}\text{-V}_{\text{As}}$  antisite-vacancy pair has no charge state that shows any similarity with the hf interactions of the defect observed experimentally. However, results obtained theoretically for the nearest-neighbor  $(\text{As}_{\text{Ga}}\text{-Ga}_{\text{As}})^-$  antistructure pair show all the details observed experimentally. Furthermore, the calculated pair binding energy is compatible with a defect that is stable up to 500–550 K. For the other two defects the identification is still unclear: The hf interactions obtained experimentally for the  $\text{As}_{\text{Ga}}\text{-X}_1$  defect agree in nearly all details with theoretical results obtained for the distant  $(\text{As}_{\text{Ga}}\text{-Ga}_{\text{As}})^-$  antistructure pair. However, the calculated shf interaction with the antisite nucleus is much smaller than the observed interaction with a single Ga nucleus. In the theoretical results there is a shf interaction of the magnitude observed experimentally, however, for a shell consisting of two equivalent nuclei. In all cases considered, shf interactions with Ga nuclei of the order of 20 MHz occurred for distant ligands only, but not with the  $\text{Ga}_{\text{As}}$  antisite nucleus. We therefore have no real evidence that the  $\text{As}_{\text{Ga}}\text{-X}_1$  defect does indeed involve an  $\text{Ga}_{\text{As}}$  antisite. From the experiment it can be concluded that it is no tetrahedral defect and that the first shell of ligands of the  $\text{As}_{\text{Ga}}$  defect consists of four As ligands.

For the technologically important EL2 defect the  $\text{As}_{\text{Ga}}\text{-As}_i$  model can be excluded on the basis of recent high-field ODENDOR experiments.<sup>29</sup> Since a slight but definite deviation from tetrahedral symmetry is observed in these experiments, it appears that this thermally most stable defect in the  $\text{As}_{\text{Ga}}$  family is some defect aggregate. We have not found an example for a defect, which, upon pairing with some other defect gains about 2 eV in pair binding energy, but has shf interactions that deviate from those of the isolated defect by 1.5%. We have proposed as a likely solution to this paradox a model in which near room temperature the EL2 is an isolated tetrahedral defect and that the deviations from tetrahedral symmetry observed experimentally are caused by the pairing with some other mobile defect, shallow acceptors on the Ga sublattice, e.g., which occurs while cooling the sample.

\*Electronic address: h.overhof@phys.upb.de

†Electronic address: martin@family-spaeth.de

- <sup>1</sup>F. K. Koschnick and J.-M. Spaeth, Phys. Status Solidi B **216**, 817 (1999).
- <sup>2</sup>J. Dabrowski and M. Scheffler, Phys. Rev. Lett. **60**, 2183 (1988); J. Dabrowski and M. Scheffler, Phys. Rev. B **40**, 10391 (1989).
- <sup>3</sup>D. J. Chadi and K. J. Chang, Phys. Rev. Lett. **60**, 2187 (1988); Phys. Rev. B **39**, 10063 (1988).
- <sup>4</sup>D. J. Chadi, Phys. Rev. B **68**, 193204 (2003).
- <sup>5</sup>K. Krambrock, J.-M. Spaeth, C. Delerue, G. Allan, and M. Lannoo, Phys. Rev. B **45**, 1481 (1992).
- <sup>6</sup>K. Krambrock and J.-M. Spaeth, Mater. Sci. Forum **83/87**, 887 (1992).
- <sup>7</sup>J.-M. Spaeth and K. Krambrock, in *Festkörperprobleme/ Advances in Solid State Physics*, edited by R. Helbig (Vieweg, Braunschweig, 1994), Vol. 33, p. 111.
- <sup>8</sup>D. E. Holmes, R. T. Chen, K. R. Elliott, and C. G. Kirkpatrick, Appl. Phys. Lett. **40**, 46 (1982).
- <sup>9</sup>M. K. Nissen, A. Villemaire, and M. L. W. Thewalt, Phys. Rev. Lett. **67**, 112 (1991).
- <sup>10</sup>J. Lagowski, H. C. Gatos, C. H. Kang, M. Skoronski, K. K. Ko, and D. G. Lin, Appl. Phys. Lett. **49**, 892 (1986).
- <sup>11</sup>O. Gunnarsson, O. Jepsen, and O. K. Andersen, Phys. Rev. B **27**, 7144 (1983).
- <sup>12</sup>J.-M. Spaeth and H. Overhof, *Point Defects in Semiconductors and Insulators* (Springer-Verlag, Heidelberg, 2003), Chap. 8.
- <sup>13</sup>G. A. Baraff and M. Schlüter, Phys. Rev. Lett. **55**, 2340 (1985).
- <sup>14</sup>C. Delerue, Phys. Rev. B **44**, 10525 (1991).
- <sup>15</sup>K. Elliot, R. T. Chen, S. G. Greenbaum, and R. J. Wagner, Appl. Phys. Lett. **44**, 907 (1988).
- <sup>16</sup>U. Gerstmann and H. Overhof, Physica B **308-310**, 561 (2001).
- <sup>17</sup>K. H. Wietzke, Ph.D. Dissertation, Paderborn, 1997.
- <sup>18</sup>H. J. von Bardeleben, J. C. Bourgoin, and A. Miret, Phys. Rev. B **34**, 1360 (1986).
- <sup>19</sup>F. K. Koschnick, K.-H. Wietzke, and J.-M. Spaeth, Phys. Rev. B **58**, 7707 (1998).
- <sup>20</sup>S. Pöykkö, M. J. Puska, M. Alatalo, and R. M. Nieminen, Phys. Rev. B **54**, 7909 (1996).
- <sup>21</sup>R. J. Wagner, J. J. Krebs, G. H. Strauss, and A. M. White, Solid State Commun. **36**, 15 (1980).
- <sup>22</sup>M. Kaminska, M. Skowronski, and W. Kuszko, Phys. Rev. Lett. **55**, 2204 (1985).
- <sup>23</sup>B. K. Meyer, J.-M. Spaeth, and M. Scheffler, Phys. Rev. Lett. **52**, 851 (1984).
- <sup>24</sup>H. J. v. Bardeleben, D. Stiévenard, and J. C. Bourgoin, Appl. Phys. Lett. **47**, 970 (1985).
- <sup>25</sup>H. J. von Bardeleben, C. Delerue, and D. Stiévenard, Mater. Sci. Forum **143-147**, 223 (1994).
- <sup>26</sup>B. K. Meyer, D. M. Hofmann, J. R. Niklas, and J.-M. Spaeth, Phys. Rev. B **36**, 1332 (1987).
- <sup>27</sup>C. Delerue, M. Lannoo, D. Stiévenard, H. J. von Bardeleben, and J. C. Bourgoin, Phys. Rev. Lett. **59**, 2875 (1987).
- <sup>28</sup>F. Wirbeleit and J. R. Niklas, Mater. Sci. Forum **258-263**, 987 (1997).
- <sup>29</sup>I. Tkach, K. Krambrock, H. Overhof, and J.-M. Spaeth, Physica B **340-342**, 353 (2003).
- <sup>30</sup>H. Overhof and J.-M. Spaeth, Physica B **340-342**, 304 (2003).